Aerodynamic Performance of Straight-Bladed Vertical Axis Wind Turbines: A Practical Open Source Implementation

Alejandro J. Vitale[1,2,3‡], Sibila A. Genchi[2,4], Andrea P. Rossi[2,3,5], Eduardo D. Guillermo[2,5], Horacio R. di Prátula[2,5]

[1]Instituto Argentino de Oceanografía (IADO), CC 804, B8000FWB, Bahía Blanca, Argentina

[2]Grupo de Estudio Sobre Energía (GESE), Universidad Tecnológica Nacional Facultad Regional Bahía Blanca, 11 de Abril 461, B8000LMI, Bahía Blanca, Argentina

[3]Departamento de Ingeniería Eléctrica y de Computadoras, Universidad Nacional del Sur, 8000 Bahía Blanca, Argentina

[4]Departamento de Geografía y Turismo, Universidad Nacional del Sur, 8000 Bahía Blanca, Argentina

[5]Departamento de Ingeniería Eléctrica, Universidad Tecnológica Nacional Facultad Regional Bahía Blanca, 8000 Bahía Blanca, Argentina

(vitale.alejandro@gmail.com, sibila.genchi@uns.edu.ar, aprossi@frbb.utn.edu.ar, eguiller@frbb.utn.edu.ar, hrdiprat@frbb.utn.edu.ar)

‡Corresponding Author; Alejandro J. Vitale, IADO: La Carrindanga Km 7,5, CC 804, B8000FWB, Bahía Blanca, Argentina, Tel: +54 291 4861666-157, vitale.alejandro@gmail.com

Received: 03.08.2017 Accepted:18.10.2017

Abstract- This study presents a practical open source implementation that uses double-multiple streamtube model for the aerodynamic performance prediction of straight-bladed vertical axis wind turbines, particularly, the power coefficient (*Cp*) and tip speed ratio (λ) relationship. To improve the analytical capability of the proposed implementation, important aspects of performance such as dynamics stall and, fixed/variable pitch blade were added. In addition, a fast convergence method for finding the axial induction factor was adopted, giving simplicity to the implementation. Simulated $Cp(\lambda)$ curves were compared with the experimental data (wind tunnel and field) reported in the literature. The mean absolute error of the simulated $Cp(\lambda)$ curves, in terms of efficiency, was 0.06, with a mean maximum of 0.078 and a mean minimum of 0.047. The good agreement in combination with the low computing time, suggests that the proposed implementation provides a useful tool for predicting aerodynamic properties of the straight-bladed vertical axis wind turbines and, therefore, for its design. The implementation can be carried out successfully by using GNU-Octave.

Keywords Straight-bladed vertical axis wind turbine, double-multiple streamtube, power coefficient, open source.

1. Introduction

The great increase in energy demand, the rising fossil fuel prices, as well as the urgency to provide a fast response to the climate change caused by the greenhouse gas emissions associated with the electrical sector [1],[2], led many countries to exploit renewable energy sources. In this context, wind is considered to be among of the most promising alternatives for the energy supply [3], because it implies inexhaustible and clean energy source. In fact, according to the Renewables 2016 - global status report [4], of the total global installed renewable electric capacity (not including hydropower) of 785 GW, about 55 % is originated from wind power.

There is a growing interest in the use of vertical axis wind turbine (VAWT), which has the potential to reduce

wind energy costs [5]. VAWT can work even in unstable wind conditions [6], making them suitable for urban and small-scale applications [7]. Among the VAWT types, the straight-bladed (SB) VAWT (also called H-rotor) is the simplest type, offering a significant advantage in terms of construction, maintenance and cost [8]. VAWTs have some disadvantages associated with the poor self-starting ability that can be avoided by careful design [9]. The key is to find the optimal design parameters of the turbine rotor blade in order to increase considerably the performance of the VAWTs, reaching a level comparable to that of horizontal axis turbines.

The optimum operating conditions (i.e., maximum power coefficient) of a wind turbine depend on the rotor solidity and the tip speed ratio [10]. Power coefficient (*Cp*) versus tip speed ratio (λ) curve is used to describe the aerodynamic properties of the rotor blade, particularly for modelling the torque production at different flow speeds [11]. Any deviation of the expected relation between these variables has an important economic impact [12]. The *Cp(λ)* curve is often difficult to obtain, requiring wind tunnels or field experiments, or complex computational fluid dynamics calculations. As an alternative to this, the use of blade element - momentum (BEM) models for the design and analysis of VAWT increased in the literature due to the acceptable accuracy of their results [13]. Based on BEM theory, aerodynamic streamtube models were evolving and adapting to different computational technologies. At present, one of the most widely used streamtube models is that developed by Paraschivoiu in 1981 [14], which involves a multiple streamtube system divided into two parts (i.e., double-multiple streamtube (DMS)), where the upwind and downwind components of the induced velocities at each level of the rotor are calculated by using the principle of two actuator disks.

The previous researches on VAWTs are less numerous than those of the horizontal axis turbines. In this context, there are few available computer tools for designing and simulating VAWTs when compared to the numerous tools that exist for horizontal axis turbines [15]. We can cite the work of Marten *et al.* [15], who carried out a review of the most prominent tools that model VAWT, which were divided into two groups: aerodynamic and structural. Within the former group, the most common computer codes based on DMS model were developed by Paraschivoiu in the 80's, which evolve three generations: CARDAA, CARDAAV and CARDAAX. However, computer codes for VAWT analysis that are reliance on readily available in the form of open source is difficult to be found.

It is precisely the limitation outlined immediately above that determines the motivation of this study. The use of open source implementation in aerodynamic designs optimization is increasingly becoming dominant, particularly when considering the high time-cost of production of wind turbine rotor prototypes and the difficulty to obtain experimental data. In this work, a practical implementation code in the form of open source MATLAB script that uses DMS model is fully presented to simulate the *Cp(λ)* curve for SB-VAWT aimed to allow scientific researches and developers to design and also to evaluate the performance of well-known rotors in different situations. In order to improve the analytical capability of this implementation, fixed and variable pitch and dynamic stall mechanisms involved in the performance were added. In addition, a fast convergence method for finding the axial induction factor was adopted, giving simplicity to the implementation.

2. Implementation Description

2.1. Basic Theory

In the DMS model, the rotor swept area (*A*) is divided into two sections along the incoming flow (U_∞): upstream (*u*) and downstream (*d*) (Fig. 1). The rotor is partitioned into a number of streamtubes (Fig. 1); the principle of momentum conservation is applied in each streamtube. The mathematical development concerning DMS model was explained in greater detail elsewhere (e.g., Freris [16], Burton *et al.* [17] and Manwell *et al.* [18]). In this work, we only present the basic equations required to solve the system.

The tip-speed ratio (λ) is defined as:

$$\lambda = \frac{R\Omega}{U_\infty} \tag{1}$$

where *R* is the rotor radius and Ω is the angular velocity (Fig. 1).

The local relative flow velocity in the upstream (W_u) and downstream (W_d) sections is given by [16]:

$$(W_u)^2 = (\Omega R + U_u(1-a_u)\sin(\theta))^2 + (U_u(1-a_u)\cos(\theta))^2 \tag{2}$$

$$(W_d)^2 = (\Omega R + U_d(1-a_d)\sin(\theta))^2 + (U_d(1-a_d)\cos(\theta))^2 \tag{3}$$

where U_u and U_d are the flow velocities in the upstream and downstream sections, respectively; a_u and a_d are the axial induction factors in the two sections, and θ is the azimuth angle (Fig. 1).

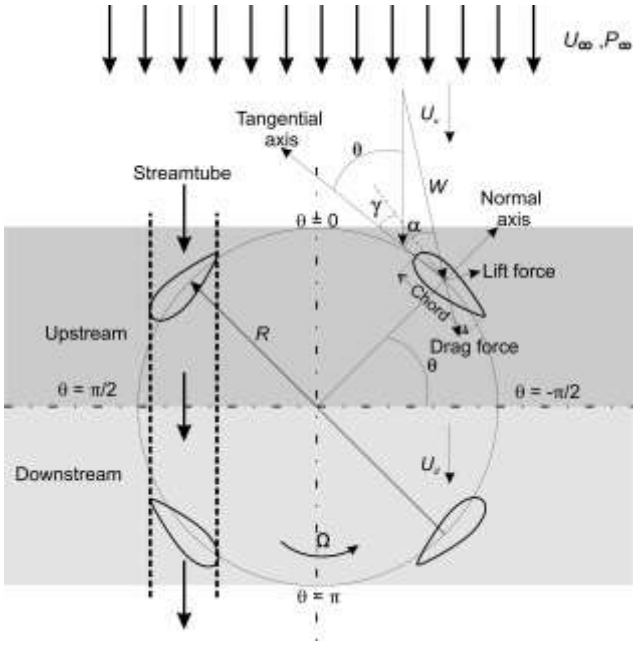

Fig. 1. Synthetic scheme showing the forces exerted on an airfoil, the DMS and the flow vectors at upstream and downstream.

The angle of attack in the upstream (α_u) and downstream (α_d) sections is determined geometrically as:

$$\alpha_{\mathrm{u}} = tg^{-1}\left(\frac{U_u(1-a_u)\cos(\theta)}{(\Omega R + U_u(1-a_u)\sin(\theta))}\right) \quad (4)$$

$$\alpha_{\mathrm{d}} = tg^{-1}\left(\frac{U_d(1-a_d)\cos(\theta)}{(\Omega R + U_d(1-a_d)\sin(\theta))}\right) \quad (5)$$

If we consider the blade pitch angle ($\gamma(\theta)$) correction (α_{upc}, α_{dpc}), we have the following equations:

$$\alpha_{\mathrm{upc}} = \alpha_{\mathrm{u}} - \gamma(\theta) \quad (6)$$

$$\alpha_{\mathrm{dpc}} = \alpha_{\mathrm{d}} - \gamma(\theta) \quad (7)$$

The flow around the blade is not steady; therefore, a dynamic stall model was considered to correct stall conditions. We used the Boeing-Vertol dynamic stall model [19] as modified by Strickland [20] which provides a good estimation (see Paraschivoiu and Allet [21]). This model assumes that the lift-curve slope and zero-lift angle remain unchanged, and that dynamic effects only modify the angle of attack at which stall occurs [20]. The model is used for the low-turbulence zone only (i.e., θ = 135° to 15°).

The values of lift stall (y_L) and drag stall (y_D) are calculated by:

$$y_L = (1.4 - 6(0.06 - t/c))\left(\frac{\pi}{180}\right) \quad (8)$$

$$y_{\mathrm{D}} = (1 - 2.5(0.06 - t/c))\left(\frac{\pi}{180}\right) \quad (9)$$

where t/c is the blade relative thickness.

The K_1 (empirical constant) values change with the sign of the effective angle of attack $S_{\alpha(u,d)}$ and are given by [20]:

$$K_1 = 0.75 + 0.25 S_{\alpha(u,d)} \quad (10)$$

A modified angle of attack is used for entering lift ($\alpha_{(u,d)pcL}$) and drag ($\alpha_{(u,d)pcD}$) data by the following relation:

$$\alpha_{(u,d)pcL} = \alpha_{(u,d)pc} - \gamma_L K_1 \sqrt{\left|\frac{\dot{c\alpha}_{u,d}}{2W_{u,d}}\right|} S_{\alpha(u,d)} \quad (11)$$

$$\alpha_{(u,d)pcD} = \alpha_{(u,d)pc} - \gamma_D K_1 \sqrt{\left|\frac{\dot{c\alpha}_{u,d}}{2W_{u,d}}\right|} S_{\alpha(u,d)} \quad (12)$$

where $\dot{c\alpha}_{u,d}$ represents the instantaneous rate of change of blade angle of attack, and c is the blade chord (m).

The thrust in the upstream (F_u) and downstream (F_d) sections at different azimuthal positions can be expressed as [16]:

$$F_u = \frac{Nc}{8\pi R}\frac{W_u^2}{U_u^2}\sec(\theta)(Cn_u\cos(\theta) - Ct_u\sin(\theta)) \quad (13)$$

$$F_d = \frac{Nc}{8\pi R}\frac{W_d^2}{U_d^2}\sec(\theta)(Cn_d\cos(\theta) - Ct_d\sin(\theta)) \quad (14)$$

where N is the number of blades; c must be corrected according to the blade chord pitch ($c = c_o\cos(\gamma)$, where c_o is the blade chord at $\gamma(\theta)$). Cn and Ct are the normal and tangential coefficients, respectively, at an angle of attack ($\alpha_{u,d}$). These coefficients, which are related to the lift (Cl) and drag (Cd) coefficients at an angle of attack $\alpha_{upcL,D}$ or $\alpha_{dpcL,D}$, are defined as:

$$Cn = [Cl\cos(\alpha) + Cd\sin(\alpha)] \quad (15)$$

$$Ct = [Cl\sin(\alpha) - Cd\cos(\alpha)] \quad (16)$$

Since the momentum equation is not applicable beyond axial induction factor of a_T, an empirical formula (called Glauert empirical correction) is used to calculate the thrust in the upstream and downstream sections [16],[17],[18], which is expressed as follows:

$$\begin{cases} F = a(1-a), a < a_T & (17) \\ F = C_{T1} - 4(\sqrt{C_{T1}} - 1)(1-a), a \geq a_T & (18) \end{cases}$$

where a_T is given by:

$$a_T = 1 - 1/2\sqrt{C_{T1}} \quad (19)$$

and C_{T1}=1.816 [17]. From Eqs. (13-14) and (17-18), the desired error (e) is defined as:

$$e = |F - F_{u,d}| \quad (20)$$

The tangential force coefficient for each streamtube in the upstream (Ft_u) and downstream (Ft_d) sections is defined as:

$$Ft_u = Ct_u\left(\frac{W_u}{U_\infty}\right)^2 \quad (21)$$

$$Ft_d = Ct_d\left(\frac{W_d}{U_\infty}\right)^2 \quad (22)$$

The torque per unit of length for each streamtube (Q_i) and for the whole rotor (Q_T) are given by the following equations [16]:

$$Q_i = 1/2\frac{Nc\rho}{2\pi(U_u + U_d)}\left(W_u^2U_d\left(Ct_uR + Cn_u\frac{c}{4}\right) + W_d^2U_u\left(Ct_dR + Cn_d\frac{c}{4}\right)\right)\Delta\theta \quad (23)$$

$$Q_T = L\sum_{\theta=-\frac{\pi}{2}}^{\theta=\frac{\pi}{2}} Q_i \quad (24)$$

where ρ is the fluid density and L is the rotor length.

The power generation (P) and Cp are defined as:

$$P = Q_r\Omega \quad (25)$$

$$Cp = \frac{P}{1/2\,\rho U_\infty^3 A} \quad (26)$$

2.2. Numerical Procedure

The flowchart presents the step-by-step procedure to obtain the $P(\Omega)$ and, therefore, $Cp(\lambda)$ curve, following the DMS model (Fig. 2). The flowchart must be read together with above-mentioned equations and MATLAB code (Appendix). The primary flowchart is displayed at the left, while the remaining part shows a detailed procedure to find the axial induction factor.

We calculated the solutions for each streamtube (upstream-downstream sections) at blade azimuth positions in the range $\theta = -\pi/2$ to $\pi/2$ by iteration until the convergence is achieved (Figs. 1 and 2). Once the convergence is achieved, the implementation is ready to run all subsequent calculations (i.e., torque and power).

3. Results and Discussion

It should be added that the implementation was performed under a set of boundary conditions that are modifiable. For instance, we calculate solutions for each streamtube at $\Delta\theta = 0.05$ rad increments. From the difference between $F_{u,d}$ (Eqs. (13-14)) and F (Eqs. (17-18)), we set a desired error of 0.01 %. Aerodynamic data concerning Cl and Cd curves (α from $-\pi$ to π) were obtained from XFLR5 software [22] and Sheldahl and Klimas [23]. The remaining boundary conditions were obtained from experiments (e.g., wind velocity, rotor parameters).

3.1. Validation Results

In order to validate the implementation, a set of wind tunnel and field experimental tests reported in the literature: Bravo *et al.* [24], Howell *et al.* [25], Raciti Castelli *et al.* [13] and Kjellin *et al.* [5] were considered, which involve different blade and rotor characteristics. A description of the considered turbine rotors (TR) is summarized in Table 1.

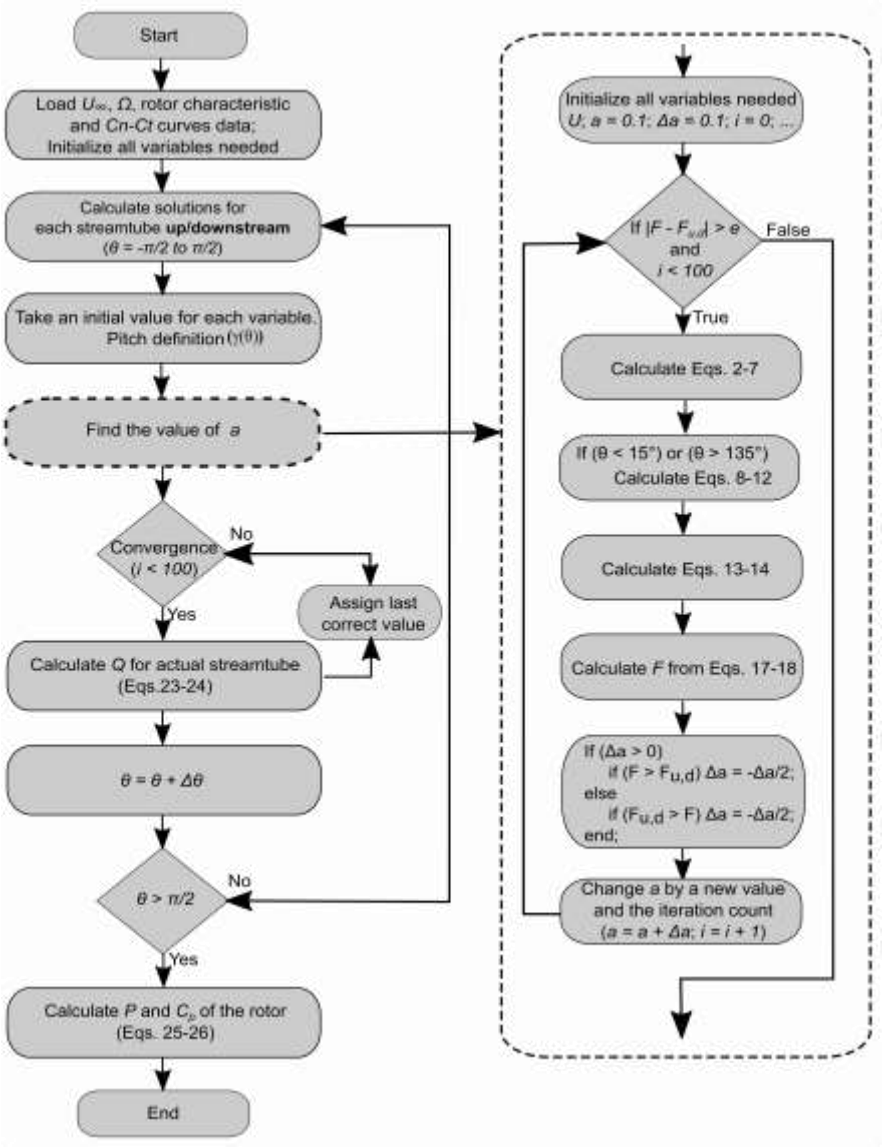

Fig. 2. Flowchart illustrating the steps to obtain the $P(\Omega)$.

Table 1. Description of the turbine rotors available in the literature that were used in this study

Publication Data[1]	Rotor radius (m)	Rotor Length (m)	Blade chord (m)	Number of blades	Blade airfoil
Bravo *et al.* [[24]](TR1)	1.25	3	0.4	3	NACA0015
Howell *et al.* [[25]] (TR2)	0.3	0.4	0.1	3	NACA0022
Raciti Castelli *et al.* [[13]] (TR3)	0.515	1.456	0.0858	3	NACA0021
Kjellin *et al.* [[4]] (TR4)	3	5	0.25	3	NACA0021

[1] All TRs have a fixed pitch of 0°.

The Figure 3 shows the validation of simulated *Cp(λ)* curves belonging to different turbine rotors (Table 1), based on available experimental tests (wind tunnel and field). The mean absolute error of the *Cp* for all simulated curves was 0.06. Simulated *Cp(λ)* curves of TR1 and TR4 showed the highest (0.078) and lowest (0.047) mean absolute error, respectively.

The behaviour between simulated and measured *Cp(λ)* curves was different in each case (TR), which indicates the absence of any bias effect (Fig. 3). For instance, there was a case (TR4) in which the simulated *Cp(λ)* curve was slightly overestimated, resulting in average 0.056; in the remaining cases (TR1,2 and 3), the simulated data were underestimated (Fig. 3). In reference to the TR1 and TR2, the simulated curves were shifted less than 0.3 *λ* (maximum *Cp* values). On the other hand, it is important to note that, at maximum *Cp* values, the absolute error tends to decrease in almost all simulations.

Therefore, the simulated *Cp(λ)* curves follow, to a large degree, the trend of the experimental data. The latter is especially important over the operating points of maximum power, which is key to the adaptation and design process of a turbine.

3.2. Computing Time

We evaluated the computing time of the implementation, which was measured by using MATLAB (R2014a) clock function at AMD Phenom II X6 processor 2.80GHz, with 64-bit operating system. The measurements were made several times for every specific run (e.g., desired error, azimuth angle step), and the average value of the measurements was used. The test, which includes all the steps in the flowchart (Fig. 2), was performed on *Cp(λ)* curves that were generate in a resolution of 100 points, based on characteristics of TR4.

A fixed step size of 0.05 rad (azimuth angle) and a desired error of 0.01 % was used, according to the considered boundary conditions. On a log scale, linear relationships were found between consuming time and both desired error and azimuth angle step (and iterations number). The maximum time for obtaining the best results at 0.001 % error and at 0.01 rad (azimuth angle step) was 40 s and 280 s, respectively (Fig. 4). All tests showed very little computing effort, representing an important advantage to accomplish the design of a turbine.

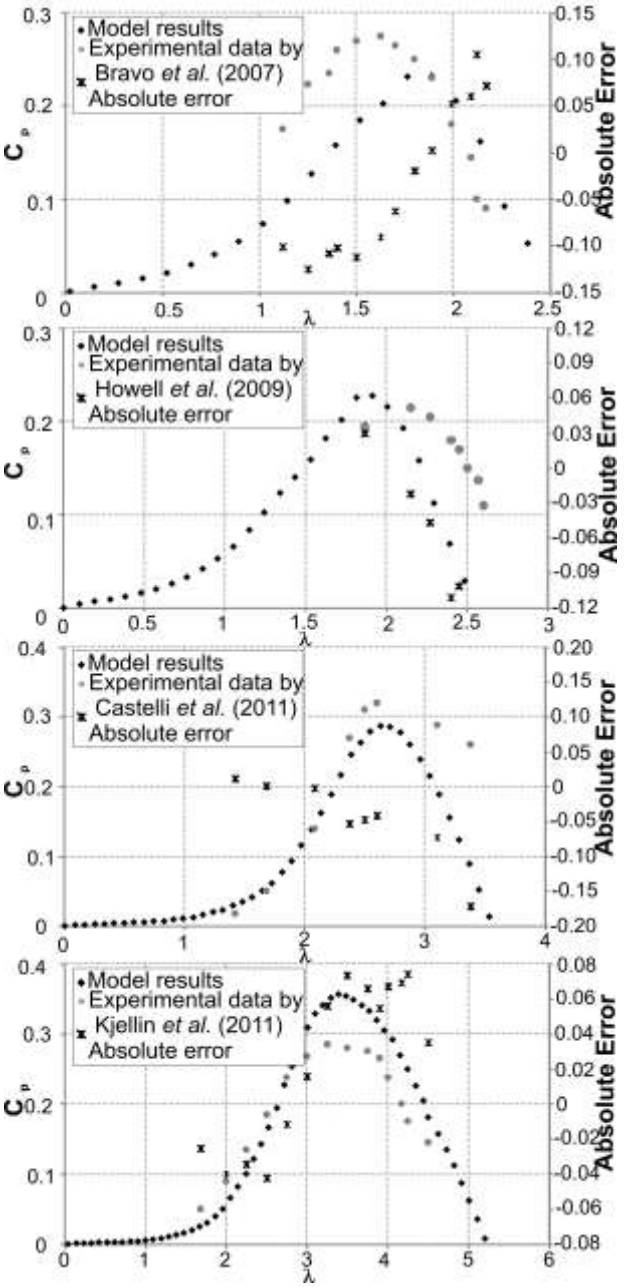

Fig. 3. Validation of simulated *Cp(λ)* curves according to the experimental data.

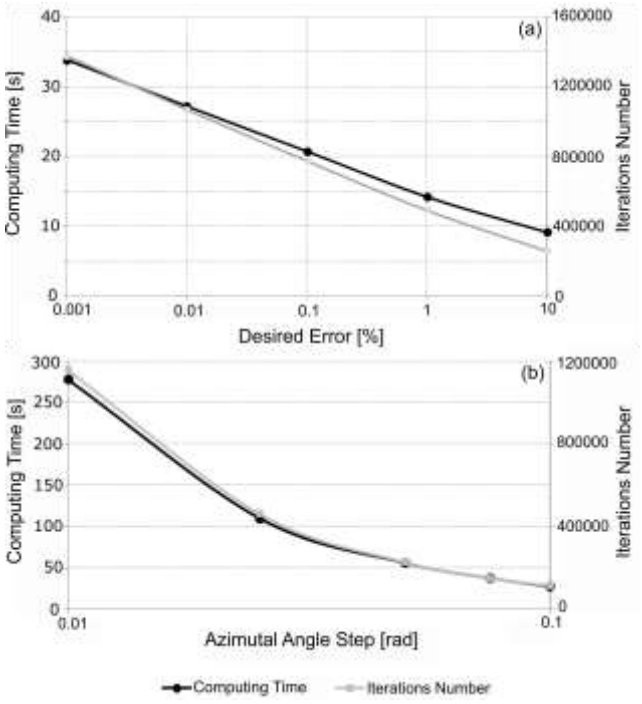

Fig. 4. Computing time of the implementation according to desired error (%) (a) and azimuthal angle step (b). Also, the convergence number can be seen in (b). Linear scale for the y-axis, and logarithmic scale for the x-axis were used.

3.3. Simulation Results and Analysis

The rotor solidity (σ) is an important variable in terms of performance because it involves the effects of dimension (rotor radius), profile and number of blades [26]. Higher solidity usually indicates lower λ and lower efficiency [25]. Figure 5 presents the simulated *Cp(λ)* curves at different solidities for two rotors. In both cases, as was expected, when increasing the solidity, λ decreases; the shape of the curve becomes more flat at low solidity (and at high λ values). The wide range of solidity values allowed to know the desired solidity to which the rotor reaches its maximum *Cp* (σ = 0.25).

Other results from the implementation, based on tangential force, are shown in Fig. 6. Each plot comprises the simulation of the tangential force coefficient (Eqs. (21-22)) from -90° to 270° azimuth angle at a maximum λ, for all the examined rotors in this study (Table 1). Generally, the simulation gives suitable results in all the cases in both upstream and downstream sections. Each rotor has its own behaviour, which depends on its blade characteristics and aspect ratio (the ratio of the blade length to the radius rotor). The tangential force (coefficient) in upstream is much greater than that in downstream section. As was expected, the maximum of instantaneous tangential force occurs at an azimuth angle of ≈ 10° in upstream and ≈ 210° in downstream. In addition, the fluctuation of the tangential force coefficient seems to be more prominently displayed in downstream section. The difference in magnitude of the tangential force between both sections is explained by the significant role of the upstream section in driving the wind turbine [26].

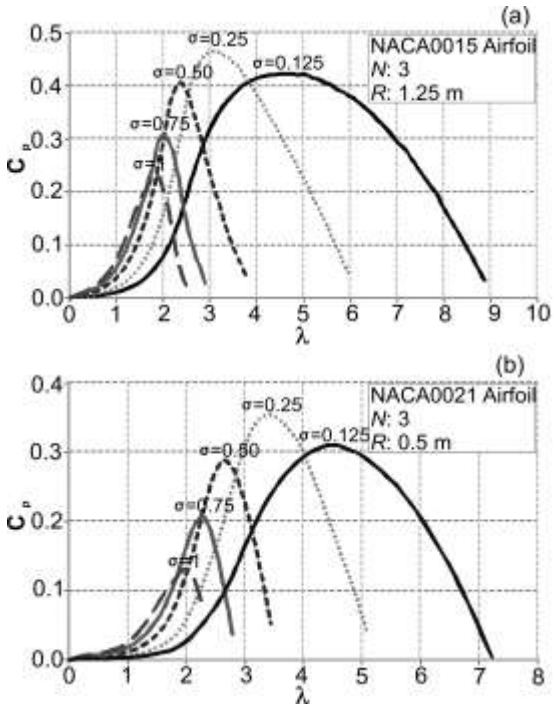

Fig. 5. Simulated *Cp*(λ) curves at different solidities (σ = 0.125 to 1) for two different rotors: TR1 (a) and TR3 (b).

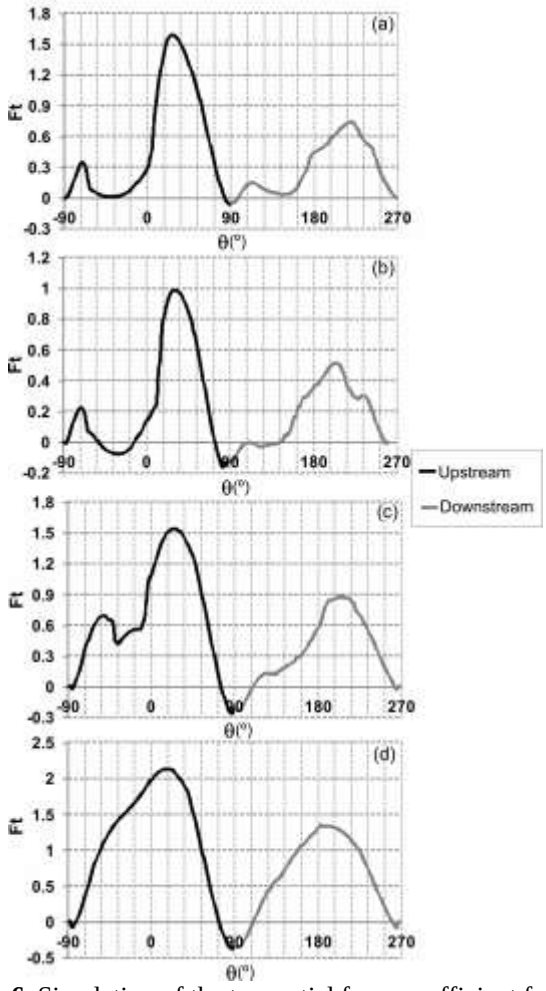

Fig. 6. Simulation of the tangential force coefficient from -90° to 270° azimuth angle at a maximum λ, in reference to TR1 (a), TR2 (b), TR3 (c) and TR4 (d) characteristics.

The performance of the TR4 (i.e., *Cp*) in several situations and with emphasis on pitch blade was computed by using the proposed implementation (Fig. 7; Tables 2-4). Figure 7 shows the performance of the TR4 at different fixed pitch blade in a range between -3 and 3°. As is shown in the figure, the maximum *Cp* (*Cp* ≈ 0.35) is achieved when the pitch angle is fixed between 0 and 2°, at $\lambda \approx 3.34$. Small changes in pitch angle (≈ 3°) caused significant decreases in the maximum *Cp* of about 20 %. Therefore, *Cp* is significantly dependent on the pitch angle. These results are in agreement with those from Mohamed *et al.* [28], in which values of pitch angle far from 0° reduce the *Cp*.

Table 2 presents the performance (maximum *Cp*) considering variable pitch angles at different amplitude levels. Clearly, the maximum efficiency decreases with increasing pitch angle amplitude. The best efficiency was observed at 1° of amplitude. This result agrees with Kiwata *et al.* [29], which found that, the *Cp* for a SB-VAWT with a small amplitude of ±3.4° (the lowest value considered) become large.

Table 3 shows the performance of an asymmetric airfoil (NACA4421) at different fixed pitch based on TR4. It can be seen that using an asymmetric airfoil, the achieved results indicated a similar trend to those in fig. 7. The maximum *Cp* is obtained at 2° (*Cp* = 0.3325, $\lambda = 3.40$).

A set of simulations were carried out in order to obtain the maximum performance (i.e, maximum *Cp*) of all considered turbine rotors (TR1 to TR4) under optimal conditions of pitch angle and rotor radius (Table 4). First, an optimal pitch angle is selected according to the original characteristics of the rotors; once found, the rotor radius is varied to obtain the best performance for each rotor. The latter is directly related to aspect ratio. As was expected, the maximum *Cp* increased significantly with decreasing aspect ratio (e.g., TR1, TR2 and TR3).

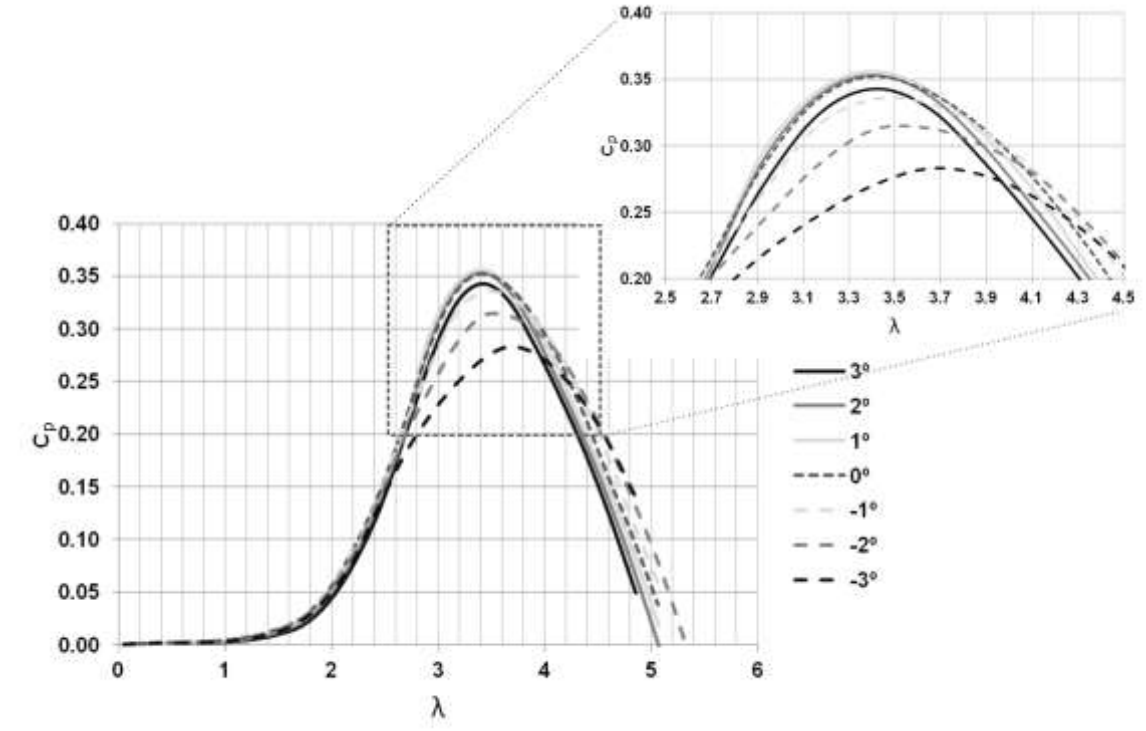

Fig. 6. Performance of the TR4 at different fixed pitch angles from -3 to 3°.

Table 2. Performance of the TR4 considering variable pitch angles $\gamma(\theta)$ at different amplitude levels

A_m(°)[1]	0°	1°	2°	3°	4°	5°
λ	3.2945	3.3974	3.4048	3.4122	3.4195	3.4269
Maximum *Cp*	0.35109	0.35217	0.34977	0.34462	0.3373	0.32616

[1] $\gamma(\theta) = |A_m \sin\theta| = |A \sin\theta|$, where A_m is the amplitude (rad).

Table 3. Performance of the TR4 considering variable pitch angles $\gamma(\theta)$ at different amplitude levels

Pitch Angle (°)	λ	Maximum *Cp*
-5°	3.4751	0.12774
-4°	3.3232	0.18715
-3°	3.2680	0.22960
-2°	3.3568	0.26291
-1°	3.3974	0.29155
0°	3.3900	0.31330
1°	3.3974	0.32698
2°	3.4048	0.33255
3°	3.4602	0.32896
4°	3.6603	0.30964
5°	3.8129	0.26823

Table4. Maximum performance (i.e, Maximum *Cp*) under optimal conditions of pitch angle and rotor radius for all considered turbine rotors

TR	Pitch Angle (°)	Rotor Radius (m)	Aspect Ratio	Maximum *Cp*	Simulated Max *Cp* of TR
TR1	0.0°	4 (1.25)	0.75 (2.40)	0.459	0.232
TR2	1.0°	1 (0.3)	0.40 (1.33)	0.425	0.226
TR3	1.5°	1 (0.515)	1.46 (2.82)	0.357	0.287
TR4	1.0°	3 (3)	1.67 (1.67)	0.356	0.352

Values in parentheses denote original values of radius (see Table 1).

4. Conclusion and Future Work

The current study provides a practical implementation following the DMS model for the performance prediction of SB-VAWT by using a code described in the appendix. Important aspects of performance, such as, dynamic stall and fixed/variable pitch angle were added to the implementation in order to evaluate alternative designs of turbine rotors. It should be noted that, unlike other studies, this study gives not only the flowchart (and associated equations) but also the MATLAB code, which is open source, fast and easy to use; and, fundamentally, the code was tested on real experimental data. The proposed implementation can be carried out successfully by using GNU-Octave.

Simulated *Cp(λ)* curves were compared with the experimental data. The mean absolute error of the simulated *Cp(λ)* curves, in terms of efficiency, was 0.06, with a mean maximum of 0.078 and a mean minimum of 0.047. The important observation is that at maximum *Cp* values, which is one of the most important parameters to determinate the power performance, the absolute error tends to decrease in almost all simulations. The good agreement between the experiment data and simulation results in combination with the little computing time (maximum time less than 280 s), suggests that the proposed implementation provides a useful tool for predicting aerodynamic properties of the SB-VAWT and, therefore, for its design. On the other hand, the implementation allows to users to carry out additional analysis of characteristic features of the VAWT such as

solidity of the rotor, tangential force coefficient, blade pitch, etc. One the most interesting results demonstrated that the maximum *Cp* is significantly dependent on the pitch angle, even with small changes. In general terms, the simulations gave suitable results, in agreement with previous findings in many cases.

Regarding future work, the latter, in conjunction with the emerging 3D printing technology, have the potential to become simple and low cost technologies for creating reliable and efficient wind turbine rotors. Another important consideration is that the same implementation can be also applied to vertical axis tidal current turbines, achieving the same kind of results, just by changing the fluid density during the setting process. The latter is important because the energy from offshore zones, which is favoured by a greater availability of wind [30], has witnessed a great expansion in the past decade [31].

Acknowledgements

This work was partly supported by the Consejo Nacional de Investigaciones Científicas y Técnicas (CONICET), the Agencia Nacional de Promoción Científica y Tecnológica and the Universidad Tecnológica Nacional Facultad Regional Bahía Blanca.

References

[1] M. Caruso *et al*., "Experimental characterization of a wind generator prototype for sustainable small wind farms," *2016 IEEE International Conference on Renewable Energy Research and Applications (ICRERA)*, Birmingham, 2016, pp. 1202-1206. doi: 10.1109/ICRERA.2016.7884523

[2] O. Charrouf, A. Betka, A. Taleb-ahmed and G. Amar, "Wind energy potential and economic analysis of WECS in four selected locations in algeria," *2016 IEEE International Conference on Renewable Energy Research and Applications (ICRERA)*, Birmingham, 2016, pp. 118-123. doi: 10.1109/ICRERA.2016.7884460

[3] A. Goudarzi, A.G. Swanson, M. Kazemi and K. Wang, "Intelligent Wind Turbine Power Curve Modelling Using the Third Version of Cultural Algorithm (CA3)", *International Journal of Renewable Energy Research*, vol.7(3), pp. 1340-1351, May 2017.

[4] REN21: Renewables 2016 Global Status Report, Frankfurt School UNEP Collaborating Centre for Climate & Sustainable Energy Finance, 2017.

[5] J. Kjellin, F. Bülow, S. Eriksson, P. Deglaire, M. Leijon, and H. Bernhoff, "Power coefficient measurement on a 12 kW straight bladed vertical axis wind turbine", *Renew. Energ.*, vol. 36(11), pp. 3050-3053, November 2011.

[6] T. Rus, L.F. Rus, A. Abrudan, F. Domnita and R. Mare, "Experimental Test in Equipping Vertical Axis Wind Turbines with Electric Generator", *International Journal of Renewable Energy Research*, vol.6(2), June 2016.

[7] S. Armstrong, A. Fiedler, and S. Tullis, "Flow separation on a high Reynolds number, high solidity vertical axis wind turbine with straight and canted blades and canted blades with fences" *Renew. Energ.*, vol. 41, pp. 13-22, May 2012.

[8] F. Ferroudji, Ch. Khelifi, and F. Meguellati, "Modal Analysis of a Small H-Darrieus Wind Turbine Based on 3D CAD, FEA", *International Journal of Renewable Energy Research*, vol.6(2), pp. 638-643, June 2016.

[9] Z. Zhao, Ch. Yang, T. Wang, B. Xu, and Y. Zheng, "Study on approach of performance improvement of VAWT employing double multiple stream tubes model", J. *Renew. Sustain. Ener.*, vol. 9, March 2017.

[10] I. Paraschivoiu, *Wind Turbine Design With Emphasis on Darrieus Concept*, Montreal: Presses Internationales Polytechnique, 2002, 423 pp.

[11] F.J. Lin, K.H. Tan, D.Y. Fang, and Y.D. Lee, "Intelligent controlled three-phase squirrel-cage induction generator system using wavelet fuzzy neural network for wind power", *IET Renew. Power Gen.*, vol. 7(5), pp. 552-564, September 2013.

[12] R.J. de Andrade Vieira and M. A. Sanz-Bobi, "Power curve modelling of a wind turbine for monitoring its behaviour", *2015 International Conference on Renewable Energy Research and Applications (ICRERA)*, Palermo, 2015.doi: 10.1109/ICRERA.2015.7418571

[13] M. Raciti Castelli, A. Englaro, and E. Benini, "The Darrieus wind turbine: Proposal for a new performance prediction model based on CFD", *Energy*, vol. 36(8), pp. 4919-4934, August 2011.

[14] I. Paraschivoiu, "Double Multiple Streamtube Model for Darrieus Wind Turbines", *2nd DOE/NASA wind turbines dynamics workshop*, Cleveland, U.S.A., pp. 19-25, February 1981.

[15] D. Marten *et al.*, "Validation and comparison of a newly developed aeroelastic design code for VAWT", *35th Wind Energy Symposium*, Texas, U.S.A., 9-13 January 2017. DOI:10.2514/6.2017-0452

[16] L.L. Freris, *Wind Energy Conversion Systems*, Hertfordshire: Prentice-Hall International, 1990, 512 pp.

[17] T. Burton, D. Sharpe, N. Jenkins, and E. Bossanyi, *Wind Energy Handbook*, New York: Wiley & Sons, 2001.

[18] J.F. Manwell, J.G. McGowan, and A.L. Rogers, *Wind Energy Explained: Theory, Design and Application*, Chichester: John Wiley & Sons, 2003.

[19] R.E. Gormont, A Mathematical model of unsteady aerodynamics and radial flow for application to helicopter rotors, *U.S. Army Air Mobility Reasearch & Development Laboratory, Vertol Division, Philadelphia*, U.S.A., 1973.

[20] J.H. Strickland, B.T. Webster, T. Nguyen, "A vortex model of the Darrieus turbine: An analytical and experimental study", *J. Fluid. Eng.*, vol. 101(4), pp. 500-505, December 1979.

[21] I. Paraschivoiu, and A. Allet, "Aerodynamic analysis of the Darrieus wind turbines including dynamic-stall effects", *J. Propulsion*, vol. 4(5), pp. 472-477, 1988.

[22] XFLR5 software. Available online: http://www.xflr5.com/xflr5.htm (accessed on 01 02 2015).

[23] R.E. Sheldahl and P.C. Klimas, Aerodynamic characteristics of seven symmetrical airfoil sections through 180-degree angle of attack for use in

aerodynamic analysis of vertical axis wind turbines, *Sandia National Laboratories*, U.S.A., 1981.
[24] R. Bravo, S. Tullis and S. Ziada, "Performance Testing of a Small Vertical-Axis Wind Turbine", *21st Canadian Congress of Applied Mechanics*, Toronto, Canada, 3-7 June 2007.
[25] R. Howell, N. Qin, J. Edwards, and N. Durrani, "Wind tunnel and numerical study of a small vertical axis wind turbine" *Renew. Energ.*, vol. 35(2), pp. 412-422, February 2010.
[26] M. Shiono, K. Suzuki, and S. Kiho, "An experimental study of the characteristics of a Darrieus turbine for tidal power generation", *Elect. Eng. Jpn.*, vol. 132(3), pp. 38-47, August 2000.
[27] L.X. Zhang, Y.B. Liang, X.H. Liu, Q.F. Jiao, and J. Guo, "Aerodynamic performance prediction of straight-bladed vertical axis wind turbine based on CFD", *Adv. Mech. Eng.*, vol. 5, April 2013.
[28] M.H. Mohamed, A.M. Ali, and A.A. Hafiz, "CFD analysis for H-rotor Darrieus turbine as a low speed wind energy converter" *Engineering Science and Technology, an International Journal*, vol. 18(1), pp. 1-13, March 2015.
[29] T. Kiwata, T. Yamada, T. Kita, S. Takata, N. Komatsu, and S. Kimura, "Performance of a vertical axis wind turbine with variable-pitch straight blades utilizing a linkage mechanism", *J. Environ. Eng.*, vol. 5, pp. 213-225, 2010.
[30] M. Beccali, J. Galletto, L. Noto and R. Provenza, "Assessment of the technical and economic potential of offshore wind energy via a GIS application: A case study for the Sicily Region according to Italian laws and incentive frameworks," *2015 International Conference on Renewable Energy Research and Applications (ICRERA)*, Palermo, 2015, pp. 1342-1347. doi: 10.1109/ICRERA.2015.7418627
[31] B. Hand, A. Cashman and G. Kelly, "An aerodynamic modelling methodology for an offshore floating vertical axis wind turbine," *2015 International Conference on Renewable Energy Research and Applications (ICRERA)*, Palermo, 2015, pp. 273-277. doi: 10.1109/ICRERA.2015.7418708

Abbreviations	
SB	Straight-bladed
VAWT	Vertical axis wind turbine
DMS	Double-multiple streamtube
BEM	Blade element-momentum
TR	Turbine rotor

Nomenclature	
Cp	Power coefficient
A	Rotor sweep area (m^2)
R	Rotor radius (m)
U_∞	Incoming flow (m s^{-1})
U	Flow velocity (m s^{-1})
W	Relative flow velocity (m s^{-1})
a	Axial induction factor
α	Angle of attack (rad)
y_L	Lift stall (rad)
y_D	Drag stall (rad)
t/c	Blade relative thickness
K_1	Empirical constant
$S_{\alpha(u,d)}$	Sign of the angle of attack
$\dot{\alpha}_{u,d}$	Instantaneous rate of change of blade angle of attack (rad s^{-1})
c	Blade chord (m)
F	Thrust
N	Number of blades
Cn	Normal coefficient
Ct	Tangential coefficient
c_o	Blade chord at $\gamma(\theta)$ (m)
Cl	Lift coefficient
Cd	Drag coefficient
C_{T1}	Empirical constant
e	Error
Ft	Tangential force coefficient
Q_i	Torque for each streamtube
Q_T	Torque for the whole rotor
L	Rotor length (m)
P	Power generation

A_m	Amplitude (rad)
σ	Rotor solidity
λ	Tip-speed ratio
Ω	Angular velocity (rad s^{-1})
θ	Azimuth angle (rad)
γ	Blade pitch angle (rad)
ρ	Fluid density (kg m^{-3})

Subscripts	
u	Upstream section
d	Downstream section
pc	Pitch corrected
pcL	Pitch corrected - lift
pcD	Pitch corrected - drag

Appendix. Source code implementation for performance predictions of straight-bladed vertical axis wind turbines.

```
function [TurbPower, TurbEfficiency, tsr, QT, Qa, THi, FTu, FTd, ...
          Nit,Nnc, APHu, APHd] = Straight_bladed_VAWT_v201705(CL,CD,PTH,...
                                                    R,L,Co,N,Om,Us,rho,tc)
```

```
%   INPUTS  %
%
%   CL, CD = Vector data for Lift and drag coefficients of the used airfoil
%   PHT    = Pitch Angle Table [rad]:
%            Example:  PTH(:,1) = -2*pi:0.1:+2*pi;
%                      PTH(:,2) = abs( 0.07*sin(PTH(:,1)) );
%   R      = Rotor radius [m]
%   L      = Blade length [m]
%   Co     = Blade chord [m]
%   N      = Numbers of blades
%   Om     = Angular velocitiy (rad/s)
%   Us     = Incoming flow [m/s]
%   rho    = Fluid density [kg/m^3]
%   tc     = t/c balde relative thickness

%
%   Last modified: May 2017
%
```

General purpose variables

```
QT          = 0;                % Torque on the complete rotor
Qa(1)       = 0;                % Azimuthal torque
FTu(1)      = 0;                % Tangential force coefficient Upstream
FTd(1)      = 0;                % Tangential force coefficient Downstream
THi(1)      = 0;                % Azimuthal positions
APHu(1)     = 0;
APHd(1)     = 0;
aphu        = pi/2;
aphd        = -pi/2;
dTh         = 0.05;             % Azimuthal differential (rad)
MAXic       = 100;              % Maximum iteration number
DA          = 0.1;              % Initial differential for induction factor (a)
dErr        = 0.0001;           % Desired error (0.01 %)
th_15       = 15  * (pi/180);   % Low-turbulence zone, border (rad)
th_135      = 135 * (pi/180);   % Low-turbulence zone, border (rad)
Yl          = (1.4-6.0*(0.06-tc))*pi/180; % lift stall, empirical constants
Yd          = (1.0-2.5*(0.06-tc))*pi/180; % Drag stall, empirical constants

% Last convergence values
au_  =DA; ad_ =DA; W2u_ =0; W2d_=0; Ctu_= 0; Ctd_= 0; Cnu_= 0; Cnd_= 0;
aphu_=0;  CPu_=0;  aphd_=0; CPd_=0;

% Glauert empirical correction coefficients (See Freris, 1990; Burton et al. 2001)
CT1 = 1.816; aT = 1 - (1/2)*(CT1^0.5);

% Iterations counter; Total iterations counter; No convergence counter;
Ni = 1; Nit = 0; Nnc = 0;
```

Main Loop

```
th0 = -pi/2 + dTh;
while ( th0 < pi/2 )

    % Upstream (udSm=1) and Downstream (udSm=2)
```

```
for (udSm=1:2)

    % Initial flow velocity Upstream
    if (udSm==1), U = Us;   end;
    if (udSm==1), th = th0; else th = pi - th0;  end;

    % Get pitch value for actual azimuth angle
    pth = interp1( PTH(:,1), PTH(:,2), th );

    % Initialize all variables needed
    a = DA; da = DA; F = 1; Fud = 0; ic = 0;

    % Determine the value of "a" for the angular velocity (?) (Eq. 13)
    while ( abs(F-Fud) > abs((F)*dErr) ) && (Fud >= 0) && (ic <= MAXic),
        %  Eqs. 2 and 3
        W2  = (Om*R + U*(1-a)*sin(th))^2 + (U*(1-a)*cos(th))^2;

        %  Four-quadrant inverse tangent (Eqs. 4 and 5)
        aph = atan2( U*(1-a)*cos(th), Om*R + U*(1-a)*sin(th) );

        % Alpha Pitch Correction  (Eqs. 6 and 7)
        aph_pc  = aph - pth;
        aph_pcL = aph_pc;
        aph_pcD = aph_pc;

        % Blade chord Pitch Correction
        C = Co*cos(pth);

        % Boeing-Vertol dynamic-stall model as modified by Strickland
        % Paraschivoiu (1988) (Eqs. 8 to 12)
        if ( (th<th_15)||(th>th_135) )
            % Sign of alpha
            Sa = -aph_pc/abs(aph_pc);

            % alpha, rate change
            if (udSm==1), Irca = ((aph-aphu)/dTh)*Om;
            else Irca = ((aph-aphd)/dTh)*Om;  end;

            % Dynamic-stall parameter
            dsp = (abs( (C*Irca)/(2*(W2^(0.5))) ))^(0.5);

            % Empirical constant
            K1 = 0.75 + 0.25*Sa;

            % Modified angle of attack alfa
            aph_pcL= aph_pc - Sa*Yl*K1*dsp;
            aph_pcD= aph_pc - Sa*Yd*K1*dsp;
        end;

        % Get Lift and Drag coefficients from "Alpha Pitch Correction"
        Cl = interp1( CL(:,1), CL(:,2), rad2deg(aph_pcL) );
        Cd = interp1( CD(:,1), CD(:,2), rad2deg(aph_pcD) );

        % Tangential and normal coefficients (Eqs. 15 and 16)
        Ct = Cl*sin(aph)-Cd*cos(aph);
        Cn = Cl*cos(aph)+Cd*sin(aph);

        % The thrust for the upstream and downstream (Eqs. 13 and 14)
        Fud = abs( ((N*C*W2)/(8*pi*R*(U^2)))*sec(th)*(Cn*cos(th)-Ct*sin(th)) );

        % Glauert empirical correction (Eqs. 17 and 18)
        if (a < aT)
            F = a*(1-a);
        else
            F = (CT1 - 4*(CT1^0.5 - 1)*(1-a)) / 4;
        end;

        % If needed, change the step for induction factor
        if (da>0)
            if (F > Fud),  da = -da/3; end;
        else
            if (Fud > F),  da = -da/3; end;
        end;

        % Induction factor increment
        a  = a + da;

        % Iteration counter
        ic = ic+1;
    end;

    % If convergence is not possible...
    if ( (Fud<0) || (ic>100) || (isnan(Fud)==1) )
        % Total No convergences counter
        Nnc   = Nnc + 1;

        % Take last correct value for this iteration
        if (udSm==1) % UpStream
            a=au_; W2=W2u_; Ct=Ctu_; Cn=Cnu_; aph = aphu_; CPu = CPu_;
        else % DownStream
            a=ad_; W2=W2d_; Ct=Ctd_; Cn=Cnd_; aph = aphd_; CPd = CPd_;
        end;
    end;
```

```
        % Results for one streamtube
        if (udSm==1) % Upstream
            %(W2^(0.5)) %Irca

            Uu = U*(1-a); W2u = W2; Ctu = Ct; Cnu = Cn; U = U*(1-2*a);
            aphu = aph; CPu = C;
            % Backup Result
            W2u_ = W2u; Ctu_= Ct; Cnu_= Cn; au_= a; aphu_ = aph; CPu_= C;
        else % Downstream
            Ud = U*(1-a); W2d = W2; Ctd = Ct; Cnd = Cn; aphd = aph; CPd = C;
            % Backup Result
            W2d_ = W2d; Ctd_= Ct; Cnd_= Cn; ad_= a; aphd_ = aph; CPd_= C;
        end;

        % Total iterations counter
        Nit = Nit + ic-1;
    end; % End loop Up/Downstream

    % Tangencial force coefficient (Eqs. 21 and 22)
    FTu(Ni) = Ctu * ( W2u / Us^2 );
    FTd(Ni) = Ctd * ( W2d / Us^2 );

    % Alpha value for each azimuth
    APHu(Ni) = aphu;
    APHd(Ni) = aphd;

    % Torque Up/Downstream (Eq. 23)
    Qa(Ni) = (N*C*rho)/(2*pi)*((W2u*Ud*(R*Ctu + Cnu*CPu/4) + ...
              W2d*Uu*(R*Ctd + Cnd*CPd/4))/(Uu+Ud))*(dTh);

    % Sum of the torque for each streamtube (Eq. 24)
    QT = QT + Qa(Ni);

    % Azimuthal increment and iteration counter increment
    THi(Ni) = rad2deg(th0);
    th0     = th0 + dTh;
    Ni      = Ni + 1;
end; % End While (Main loop)
%
QT = QT*L;
```

Function Outputs

```
mxp            = max(abs(PTH(:,2)));
R              = R*(1 + abs(C*sin(mxp)/2)); % Radius Correction
FlowPower      = rho*0.5*(Us^3)*2*R*L;      % Flow Power for Turbine area
TurbPower      = QT*Om;                     % Power turbine (Eq. 25)
TurbEfficiency = TurbPower/FlowPower;       % Coefficient power (Eq. 26)
tsr            = (Om*R)/Us;                 % Tip-speed ratio (Eq. 1)
```